Journal of Power Sources 297 (2015) 217–223

Contents lists available at ScienceDirect

Journal of Power Sources

journal homepage: www.elsevier.com/locate/jpowsour

Chromium vaporization from mechanically deformed pre-coated interconnects in Solid Oxide Fuel Cells

Hannes Falk-Windisch*, Mohammad Sattari, Jan-Erik Svensson, Jan Froitzheim

Chalmers University of Technology, Department of Chemistry and Chemical Engineering, Division of Energy and Materials, Kemivägen 10, SE-41296 Gothenburg, Sweden

HIGHLIGHTS

- Cr vaporization from real Solid Oxide Fuel Cell interconnects was measured.
- Stamping pre-coated Co coated steel induced large cracks in the coating.
- The cracks healed during exposure forming a top layer of $(Co,Mn)_3O_4$.
- As a result of the rapid healing, no increase in Cr vaporization was measured.

ARTICLE INFO

Article history:
Received 12 May 2015
Received in revised form
21 July 2015
Accepted 27 July 2015
Available online 10 August 2015

Keywords:
Interconnect
Corrosion
Coating
Vaporization
SOFC
Self-healing

ABSTRACT

Cathode poisoning, associated with Cr evaporation from interconnect material, is one of the most important degradation mechanisms in Solid Oxide Fuel Cells when Cr_2O_3-forming steels are used as the interconnect material. Coating these steels with a thin Co layer has proven to decrease Cr vaporization. To reduce production costs, it is suggested that thin metallic PVD coatings be applied to each steel strip before pressing the material into interconnect shape. This process would enable high volume production without the need for an extra post-coating step. However, when the pre-coated material is mechanically deformed, cracks may form and lower the quality of the coating. In the present study, Chromium volatilization is measured in an air-3% H_2O environment at 850 °C for 336 h. Three materials coated with 600 nm Co are investigated and compared to an uncoated material. The effect of deformation is investigated on real interconnects. Microscopy observations reveal the presence of cracks in the order of several μm on the deformed pre-coated steel. However, upon exposure, the cracks can heal and form a continuous surface oxide rich in Co and Mn. As an effect of the rapid healing, no increase in Cr vaporization is measured for the pre-coated material.

1. Introduction

High electrical conversion efficiency, clean emissions and the possibility to utilize several types of fuels, such as hydrogen and carbon-based fuels, are some of the great advantages of Solid Oxide Fuel Cell (SOFC) technology [1]. To increase the output of electricity, several cells are electrically connected in series, often referred to as a fuel cell stack. A key component in the stack is the interconnect which separates the air and fuel compartments of neighboring cells and also connects them electrically. The interconnect, also called a bipolar plate, must be gas tight, electrically conductive and stable in both high pO_2 (air on the cathode side) and low pO_2 (fuel on the anode side) environments [2,3]. Moreover, it must be shaped in a certain way that allows for gas distribution. Today, ferritic stainless steels have become the most popular choice of interconnect material for planar SOFC applications [4] that operate at 600–900 °C. The stability of such steels depends on the formation of a protective oxide that separates the oxidizing gas from the steel. Due to the requirement for good electrical conductivity of the interconnect material, steels that form a protective Al_2O_3 layer must be excluded, which leaves Cr_2O_3-forming steels as the best option. However, on the cathode side, which contains both oxygen and water vapor, Cr(VI) species, such as $CrO_2(OH)_2$, vaporize from the Cr-rich surface oxide scale [5–8]. The volatile Cr(VI) species are then transported to the cathode where they may either be reduced back to Cr(III) at the Three Phase Boundary (TPB), forming deposits which block the

* Corresponding author.
E-mail address: hannes.windisch@chalmers.se (H. Falk-Windisch).

http://dx.doi.org/10.1016/j.jpowsour.2015.07.085

electrochemical oxygen reaction process, or directly react with other stack components [9–12]. Both cases lead to fast stack degradation, and for this reason, it is of great importance to minimize Cr vaporization.

Applying ceramic or metallic coatings to reduce Cr vaporization has become the most widespread solution, and several coating systems have been studied within the last decade. One of the most promising candidates is the $(Co,Mn)_3O_4$ coating system. Such a coating can be applied utilizing various techniques such as spray drying, dip-coating, screen printing, aerosol spray deposition, plasma spraying or by Physical Vapor Deposition (PVD) [13–21]. Another alternative is to coat the steel with metallic Co which forms $(Co,Mn)_3O_4$ upon oxidation due to the outward diffusion of Mn from the steel [22–32]. Applying metallic coatings also eliminates the extra heat treatment that is necessary to produce a dense coating when techniques such as spray-drying, dip-coating and screen printing are utilized. For SOFCs to become economically attractive, their cost must be reduced significantly. Today most coated interconnect materials are manufactured in two separate steps: (1) stamping the uncoated steel into an interconnect shape and (2) coating the deformed steel plate (post-coating). This two-step batch coating concept is rather inefficient for mass production, and for this reason alternative processes should be explored. Alternatively, large amounts of steel sheet can be pre-coated and subsequently shaped into interconnects allowing for much more efficient large scale production, and as a consequence, lower overall costs. In the present study, thin PVD coatings were studied that were applied by Sandvik Materials Technology using a PVD process. With this technique several hundreds of meters can be coated in an industrial scale roll-to-roll technique enabling high volume production without the need for an extra coating step after the steel has been shaped into interconnects [33]. Earlier studies on undeformed materials have shown that thin PVD films of metallic Co significantly reduce Cr vaporization [23–26]. However, delamination of the coating as well as the formation of large cracks may occur when the pre-coated steel strip is shaped into interconnects. This may have a significant effect on Cr vaporization, which would reduce stack lifetime. For this reason, the aim of this study is to investigate whether the mechanical deformation process will lead to increased corrosion and Cr vaporization of the interconnect material.

2. Materials and methods

All exposures were performed on either uncoated or 600 nm Co coated Crofer 22 APU foils. Table 1 shows the chemical composition of Crofer 22 APU. Coatings were prepared by Sandvik Materials Technology using a Physical Vapor Deposition (PVD) process, and mechanical deformation was conducted utilizing a Topsoe Fuel Cell interconnect design. Four types of materials were analyzed: (1) uncoated and undeformed, (2) Co coated and undeformed, (3) deformed and subsequently coated (post-coated) and (4) pre-coated and subsequently deformed (see Fig. 1). Prior to exposure, all samples, with a steel thickness of 0.3 mm, were cut into 15×15 mm^2 coupons and cleaned with acetone as well as ethanol in an ultrasonic bath.

All samples were isothermally exposed to air-3% H_2O at 850 °C for up to 336 h. 850 °C was chosen as exposure temperature to accelerate the test somewhat. The flow rate was 6000 sml min^{-1} corresponding to 27 cm s^{-1}. The 3% water vapor level in the gas was achieved by bubbling dry air through a heated water bath connected to a condenser containing water at a temperature of 24.4 °C. The samples (three coupons per exposure) were placed parallel to the gas stream. Downstream of the samples, the gas was lead through a silica glass denuder tube. To collect the volatile Cr(VI) species, this denuder tube was coated with Na_2CO_3, which reacts with $CrO_2(OH)_2(g)$ according to the following reaction:

$$CrO_2(OH)_2(g) + Na_2CO_3(s) \rightarrow Na_2CrO_4(s) + H_2O(g) + CO_2(g)$$

The denuder tube could be replaced regularly and rinsed with distilled water without affecting the samples. The amount of vaporized Cr was then quantified by spectrophotometry using an Evolution 60S Thermo Scientific instrument. A more detailed description of the denuder technique and the experimental setup can be found elsewhere [25].

Mass gain was recorded as a function of time after each isothermal exposure by calculating the average mass gain from the three coupons exposed simultaneously. A six-decimal place micro balance (Metler Toledo XP6) was utilized for this purpose. The microstructure and chemical composition of each sample surface was analyzed in an FEI Quanta 200 FEG Environmental Scanning Electron Microscope (ESEM) equipped with an Oxford Instruments X-Max^N Energy Dispersive X-ray spectroscopy (EDX) detector and INCAEnergy software. High vacuum mode and an accelerating voltage of 15 kV were used for all top view images. Cross sections were prepared from two of the samples: pre-coated samples exposed for 24 h and 336 h. The cross section of the 336 h exposed sample was prepared mechanically whereas Focused Ion Beam (FIB) milling and lift-out technique were utilized to prepare a thin specimen from the pre-coated sample which had been exposed for 24 h. For this purpose, an FEI Versa 3D DualBeam Focused Ion Beam/Scanning Electron Microscope (FIB/SEM) was used. To protect the sample from ion beam damage during milling, two layers of Pt were deposited on the area of interest, first using an electron beam followed by an ion beam induced deposition. To minimize the amount of ion beam damage and amorphization, ion milling was carried out in a gradually decreasing beam current in the following steps: 850, 450 and 250 pA at 30 kV and 45 pA at 5 kV.

Table 1
Composition of the studied steel Crofer 22 APU in weight %. The values are specified according to the manufacturer for received batches.

Material	Manufacturer	Fe	Cr	Mn	Si	Ti	Add
Crofer 22 APU	ThyssenKrupp VDM	Bal.	22.9	0.38	0.01	0.06	La

3. Results and discussion

3.1. Gravimetric analysis

Mass gain and Cr vaporization, as a function of time of the isothermally exposed samples in air-3% H_2O at 850 °C, are shown in Fig. 2. All Co coated materials showed a rapid gain in mass within the first few minutes of exposure time compared to the uncoated material. This mass gain of approximately 0.2 mg cm^{-2} corresponds to oxidation of the Co coating and the formation of Co_3O_4 [24]. Furthermore, all coated samples showed similar oxidation behavior which indicates that shaping the material into an interconnect had not influenced the oxidation kinetics during the experiment period. After 336 h of exposure, all the coated materials gained 0.9–1.0 mg cm^{-2} in mass whereas the uncoated material had only gained 0.5 mg cm^{-2} in mass. The mass gain for the uncoated material after 336 h was lower than the three coated samples even when the 0.2 mg cm^{-2}, corresponding to the initial oxidation of the metallic Co coating, was compensated. The main reason for this is associated with the much higher rate of Cr vaporization for the uncoated material [24,34–36].

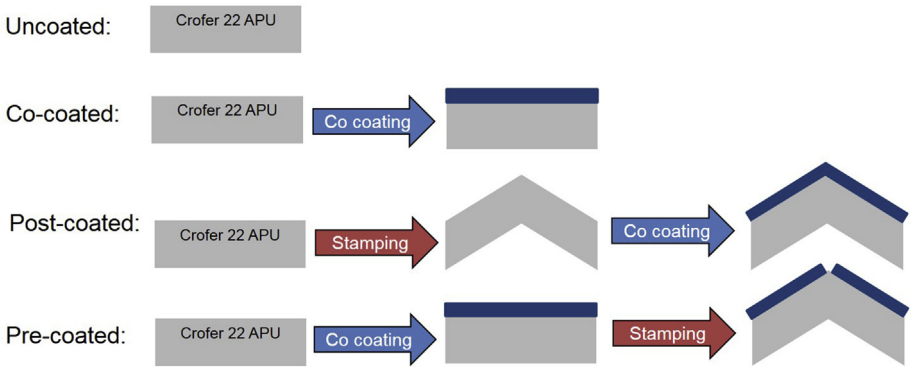

Fig. 1. Schematic drawing of the four different materials investigated.

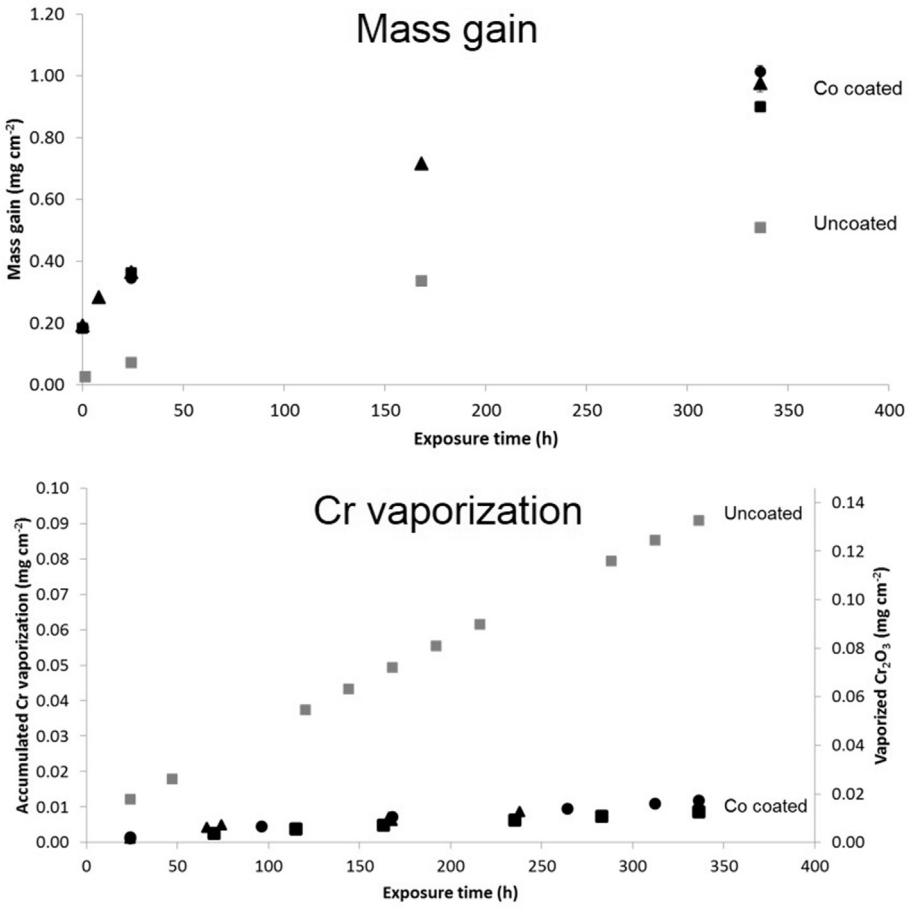

Fig. 2. Mass gain and accumulated Cr vaporization as a function of time at 850 °C in air 3% H_2O. Uncoated undeformed (grey squares); Coated undeformed (black squares); Post-coated (black dots) and Pre-coated (black triangles).

3.2. Cr vaporization measurements

Cr vaporization of the uncoated Crofer 22 APU material ($9.1*10^{-2}$ mg cm^{-2}) was significantly higher compared to all the coated materials (~$1*10^{-2}$ mg cm^{-2}). In fact, all the coated samples, including the mechanically deformed samples, showed reduced Cr vaporization by approximately 90% after 336 h. This is in good agreement with earlier studies on undeformed Co coated Sanergy HT and AISI 441 in the same exposure environment [23–26].

3.3. Microstructural investigation

The pre-coated material showed signs of crack formation after the coated steel had been pressed into an interconnect. However, these cracks were observed only where the material was subjected to the greatest amount of tensile deformation. Fig. 3 shows SEM images of various parts of the surface of the pre-coated material. From this figure, it is obvious that some areas show severe crack formation (area C) whereas other areas seem to be intact (area A). All images shown below in this paper will be from the severely deformed part (area C).

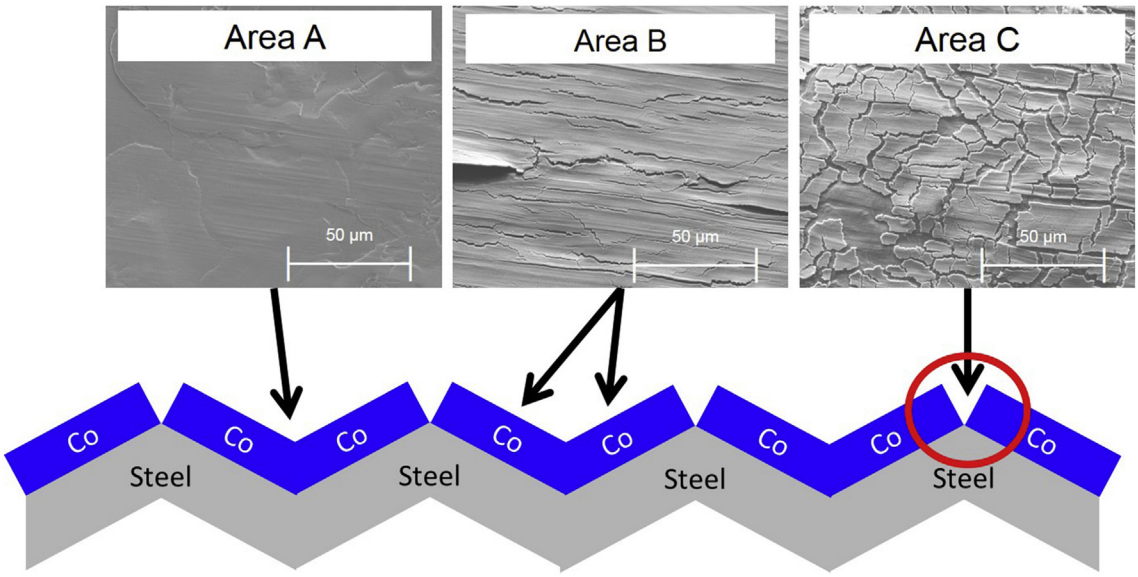

Fig. 3. SEM images from the different areas along the surface of the pre-coated material after being pressed into a real interconnect.

Fig. 4 shows the surface topography and the EDX elemental maps of both the pre- and post-coated material before exposure. It can be concluded that a dense and uniform Co coating layer is found on the post-coated material, as expected. On the pre-coated material, on the other hand, cracks in the µm-range, were formed when the pre-coated material was pressed into an interconnect. From the top view EDX elemental maps, it can be seen that the cracked areas are Fe and Cr rich and devoid of Co. This indicates that the entire coating had spalled off in the cracked area and that the detected EDX signal originated from the underlying steel substrate.

Fig. 5 shows the topography as well as the EDX elemental maps of the pre-coated material exposed for 6 min, 8 h and 24 h. After only 6 min of exposure, the metallic Co coating had been converted into a Co oxide, which is in agreement with earlier studies [24] and the mass gain observations. Oxidation of the Co coating is associated with a volume expansion of approximately a factor of two. Thus, it seems probable that small cracks may heal due to the volume expansion that takes place during the oxidation of the coating. The top view SEM micrographs and the EDX elemental maps indicate that minor cracks may have healed due to the initial volume expansion; however, most of the large cracks still remain. The EDX signal from within the cracked areas shows strong intensity for Fe and Cr and weak intensity for O, suggesting that the oxide is very thin within these areas and that most of the EDX signal has been generated within the steel.

Large cracks remain after 8 h of exposure; however, compared to after only six minutes, an enrichment of Mn can be seen in the cracked areas, most probably due to the formation of a $(Cr,Mn)_3O_4$ top layer. Earlier investigations on uncoated Crofer 22 APU or similar steels, such as Crofer 22 H, Sanergy HT and AISI 441, have shown that a double layered oxide scale consisting of an inner Cr_2O_3 layer and an outer spinel type $(Cr,Mn)_3O_4$ forms on the surface of the sample as a result of exposure in air at elevated temperatures [23,24,26,34,37,38].

After 24 h, the Fe EDX signal was very weak within the cracked areas. The Fe signal is expected to come from the steel, suggesting that the oxide scale has become thicker within the cracked area. Another significant difference is that the Cr, Mn and Co EDX signal

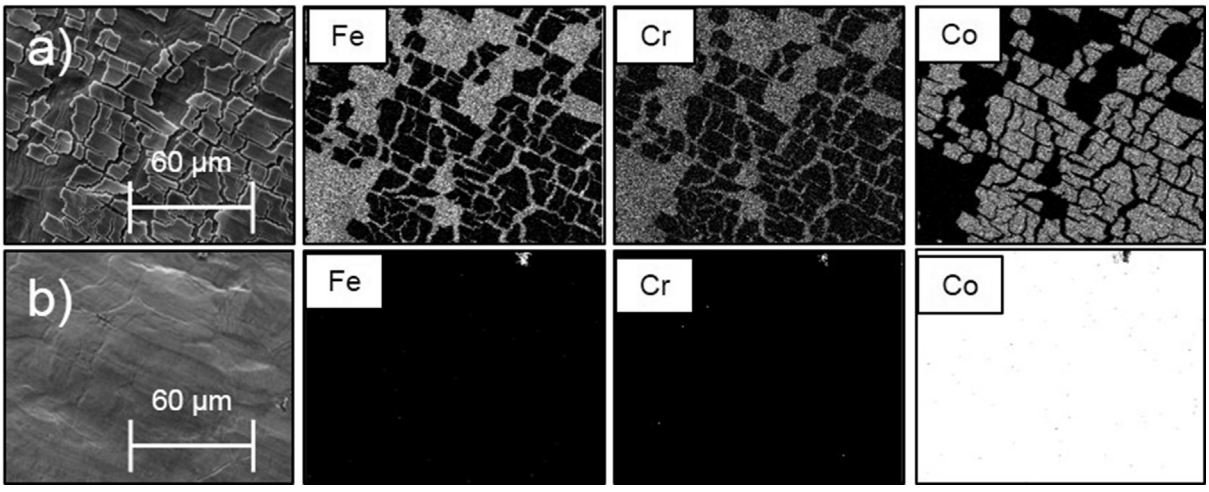

Fig. 4. Top view SEM image and EDX elemental maps before exposure for a) the pre-coated and b) the post-coated material.

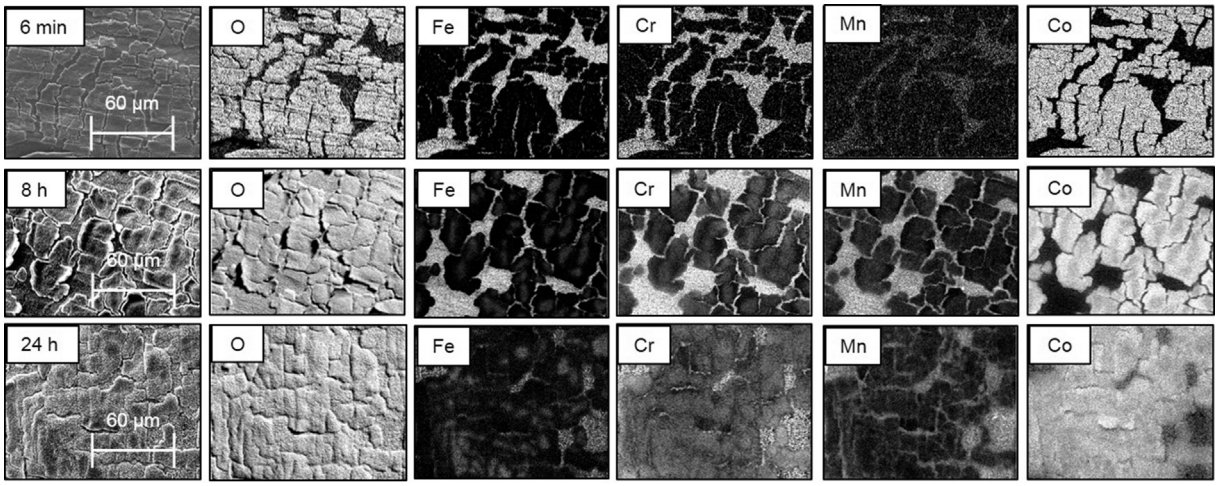

Fig. 5. Top view SEM images and EDX elemental maps for the pre-coated material after 6 min, 8 h and 24 h of exposure.

is more homogenously distributed over the surface of the sample after 24 h than after 6 min and 8 h. This becomes very clear by observing the Co signal where Co can be found within some cracked areas after 24 h. The reason for this more homogenous distribution of Cr, Mn and Co after 24 h of exposure is assumed to be an effect of interdiffusion between the Cr- and Mn-rich oxide within the cracked area and the Co-rich oxide formed when the Co coating was oxidized. If a Mn-containing steel is coated with a thin metallic Co layer, Mn will diffuse out from the steel into the oxidized Co coating during exposure and will form a $(Co,Mn)_3O_4$ layer [23,24,26]. This $(Co,Mn)_3O_4$ layer would then be in contact with the significantly thinner $(Cr,Mn)_3O_4$ layer formed in the cracked area. Interdiffusion between the two spinel type oxide scales would be expected, and consequently, the formation of an area consisting of $(Co,Cr,Mn)_3O_4$. This would explain the more homogenous distribution of Cr, Mn and Co with continued exposure time.

To enable accurate EDX analysis in the cracked area on the pre-coated sample exposed for 24 h, a thin (<200 nm) lamella was prepared using Focused Ion Beam (FIB) milling. Fig. 6 shows the area of interest from which the FIB lift-out lamella was taken, an SEM image of the thin lamella and the EDX elemental maps from this area. The EDX elemental maps from this thin lamella show that after 24 h of exposure, a continuous double layered oxide scale had been formed consisting of an inner Cr-rich layer and an outer Co- and Mn-rich top layer, which are most probably Cr_2O_3 and $(Co,Mn)_3O_4$ based on earlier investigations on the similar steel Sanergy HT coated with a thin Co coating [23,24]. Moreover, areas rich in Cr, Mn and O, probably $(Cr,Mn)_3O_4$, can be seen directly underneath the Cr_2O_3 layer. Such areas have also been observed by other authors on both Co coated and uncoated Crofer APU [22,37,39].

Although it can be concluded that the whole surface, including the cracked area, is covered by a Co-rich oxide after 24 h, a clear difference can be seen between the Co oxide within the cracked area and the Co oxide where the original Co coating was present before exposure. In the area where the Co-coating was present before exposure, the Co oxide is about 1.5–2 µm thick and the Mn concentration is low. Furthermore, large pores within the Co oxide can be observed. These pores are most probably a result of the initial oxidation of the metallic Co coating. The formation of rather large pores as an effect of fast oxidation of the Co coating has been observed earlier [24]. The Co oxide in the cracked area, on the other hand, does not contain any large pores, and the Mn content is much higher. Another difference is that the Co oxide layer within the cracked area varies significantly in thickness. It can be seen that this Co oxide consists of a very thin continuous layer and a few large cubic $(Co,Mn)_3O_4$ crystals. It is suggested that the thin continuous layer of Co oxide in the cracked area was originally a thin $(Cr,Mn)_3O_4$ top layer formed in the absence of a Co coating. This thin $(Cr,Mn)_3O_4$ layer was then transformed into a $(Cr,Co,Mn)_3O_4$ top layer with low Cr content by the interdiffusion and/or surface diffusion of Co from the Co oxide. The large cubic crystals, on the other hand, were probably not originally large $(Cr,Mn)_3O_4$ crystals transformed into chromium poor $(Cr,Co,Mn)_3O_4$ crystals. Instead, these crystals probably grew due to the interdiffusion and/or surface diffusion of Co and the outward diffusion of Mn from the steel.

With continued exposure time, the cracks observed during the first 24 h of exposure disappear (Fig. 7). Instead of cracks, the surface can be seen, in the figure, to be homogenously covered by an oxide rich in Co and Mn. The growth of rather large $(Co,Mn)_3O_4$ crystals within the cracked area could explain why no clear signs of the cracks can be seen after longer exposure times. Fig. 8 shows a cross section of the pre-coated material exposed for 336 h. It can be seen in that figure that the oxide scale after 336 h consists of an inner Cr_2O_3 layer and an outer $(Co,Mn)_3O_4$ top layer, as was the case after 24 h. Furthermore, the non-continuous oxide rich in Cr and Mn beneath the Cr_2O_3 layer seen after 24 h can also be seen in this figure after 336 h of exposure. In contrast to the 24 h sample, it can be seen that the Cr_2O_3 layer has grown thicker with continued exposure time, as expected according to the mass gain values. The chemical composition of the $(Co,Mn)_3O_4$ top layer has also changed with continued exposure time. After 24 h, a clear difference in Mn concentration was observed between the Co oxide within the cracked area and the Co oxide where the coating was present before exposure. After 336 h of exposure, in contrast, the $(Co,Mn)_3O_4$ top layer was homogenously rich in both Co and Mn, as was observed in both the top view EDX elemental maps and in the cross section (Figs. 7 and 8). Furthermore, the enrichment of Mn into the Co-oxide would lead to a volume expansion which is assumed to be the reason why the large pores observed after 24 h of exposure have disappeared with continued exposure time.

4. Conclusions

Stamping a pre-coated 600 nm Co coated Crofer 22 APU foil into an interconnect induced crack formation within the coating in certain areas of the surface of a sample. Due to quick Co diffusion;

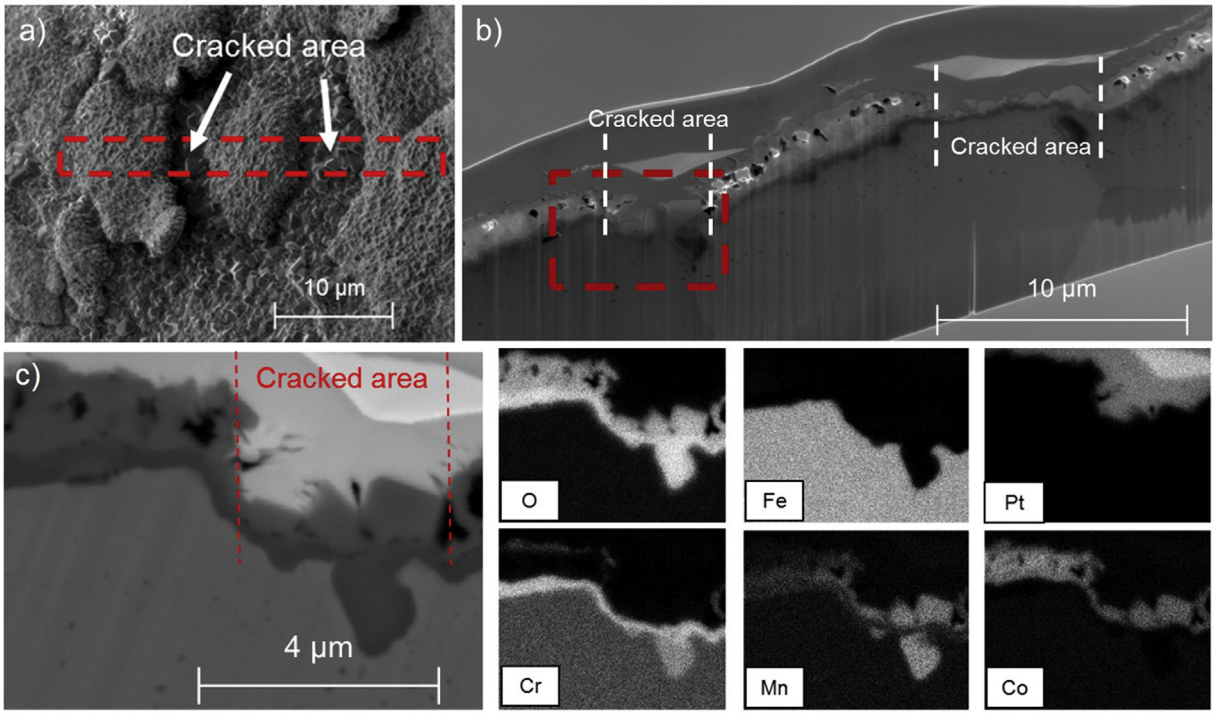

Fig. 6. a) Shows the top view SEM image of the pre-coated material exposed for 24 h. The red rectangle marks the position of the thin film lift out. In b), the SEM image of the thin lamella is shown. The area of interest for EDX mapping (red rectangle in b)) and the EDX elemental maps are shown in c). (For interpretation of the references to colour in this figure legend, the reader is referred to the web version of this article.)

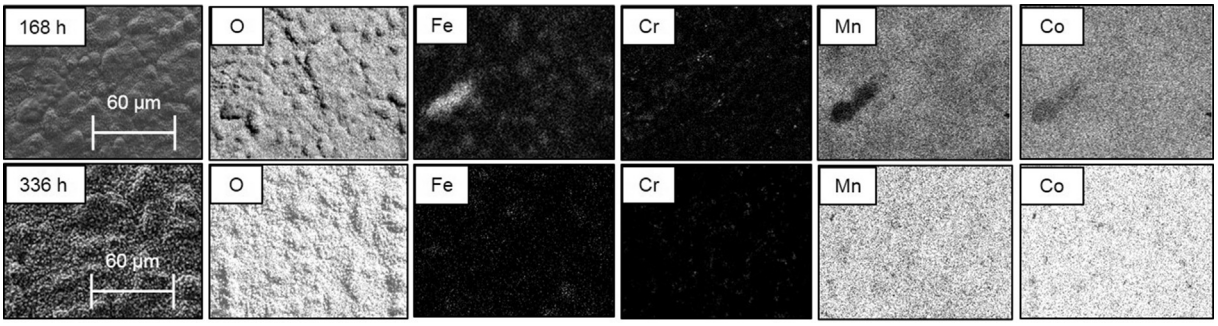

Fig. 7. Top view SEM images and EDX elemental maps for pre-coated material after 168 and 336 h of exposure.

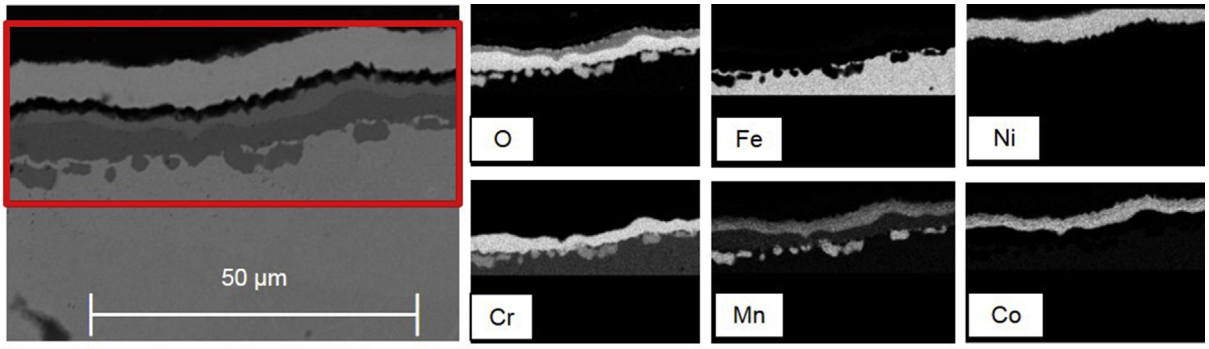

Fig. 8. SEM image and EDX elemental maps of a mechanical cross section of the pre-coated material exposed for 336 h.

however, a thin top layer of $(Co,Mn)_3O_4$ was established within the cracked area after only 24 h of exposure. The $(Co,Mn)_3O_4$ layer within the cracked area grew thicker with continued exposure time, and, after only 168 h of exposure, the surface of the pre-coated material was homogenously covered by an oxide rich in Co and Mn. As an effect of this rapid healing, no increase in Cr

vaporization was measured for the pre-coated material.

Acknowledgments

Sandvik Materials Technology is acknowledged for providing coated samples and Topsoe Fuel Cell is acknowledged for pressing them into the interconnect shape. The financial support received from the Swedish Research Council and the Swedish Energy Agency (Grant Agreement No 34140-1), The Swedish High Temperature Corrosion Centre as well as the Nordic NaCoSOFC project is gratefully acknowledged. Furthermore, the funding received from the European Union's Seventh Framework Programme (FP7/2007-2013) for the Fuel Cells and Hydrogen Joint Technology Initiative under grant agreement n°[278257] is gratefully acknowledged.

References

[1] A.B. Stambouli, E. Traversa, Renew. Sust. Energy Rev. 6 (2002) 433–455.
[2] J.W. Fergus, Mat. Sci. Eng. A Struct. 397 (2005) 271–283.
[3] W.Z. Zhu, S.C. Deevi, Mater Res. Bull. 38 (2003) 957–972.
[4] N. Shaigan, W. Qu, D.G. Ivey, W.X. Chen, J. Power Sources 195 (2010) 1529–1542.
[5] B.B. Ebbinghaus, Combust. Flame 93 (1993) 119–137.
[6] C. Gindorf, L. Singheiser, K. Hilpert, J. Phys. Chem. Solids 66 (2005) 384–387.
[7] K. Hilpert, D. Das, M. Miller, D.H. Peck, R. Weiss, J. Electrochem. Soc. 143 (1996) 3642–3647.
[8] E.J. Opila, D.L. Myers, N.S. Jacobson, I.M.B. Nielsen, D.F. Johnson, J.K. Olminsky, M.D. Allendorf, J. Phys. Chem. A 111 (2007) 1971–1980.
[9] J.W. Fergus, Int. J. Hydrogen Energy 32 (2007) 3664–3671.
[10] M.C. Tucker, H. Kurokawa, C.P. Jacobson, L.C. De Jonghe, S.J. Visco, J. Power Sources 160 (2006) 130–138.
[11] S.P. Simner, M.D. Anderson, G.G. Xia, Z. Yang, L.R. Pederson, J.W. Stevenson, J. Electrochem. Soc. 152 (2005) A740–A745.
[12] S.P.S. Badwal, R. Deller, K. Foger, Y. Ramprakash, J.P. Zhang, Solid State Ionics 99 (1997) 297–310.
[13] P.E. Gannon, V.I. Gorokhovsky, M.C. Deibert, R.J. Smith, A. Kayani, P.T. White, S. Sofie, Z. Yang, D. McCready, S. Visco, C. Jacobson, H. Kurokawa, Int. J. Hydrogen Energy 32 (2007) 3672–3681.
[14] R. Trebbels, T. Markus, L. Singheiser, J. Electrochem. Soc. 157 (2010) B490–B495.
[15] S.R. Akanda, N.J. Kidner, M.E. Walter, Surf. Coat. Technol. 253 (2014) 255–260.
[16] S.R. Akanda, M.E. Walter, N.J. Kidner, M.M. Seabaugh, Thin Solid Films 565 (2014) 237–248.
[17] B.K. Park, J.W. Lee, S.B. Lee, T.H. Lim, S.J. Park, C.O. Park, R.H. Song, Int. J. Hydrogen Energy 38 (2013) 12043–12050.
[18] Y.Z. Hu, C.X. Li, G.J. Yang, C.J. Li, Int. J. Hydrogen Energy 39 (2014) 13844–13851.
[19] N.J. Magdefrau, L. Chen, E.Y. Sun, M. Aindow, Surf. Coat. Technol. 242 (2014) 109–117.
[20] E. Alvarez, A. Meier, K.S. Weil, Z.G. Yang, Int. J. Appl. Ceram. Tec. 8 (2011) 33–41.
[21] J. Puranen, M. Pihlatie, J. Lagerbom, T. Salminen, J. Laakso, L. Hyvarinen, M. Kylmalahti, O. Himanen, J. Kiviaho, P. Vuoristo, Int. J. Hydrogen Energy 39 (2014) 17246–17257.
[22] M. Stanislowski, J. Froitzheim, L. Niewolak, W.J. Quadakkers, K. Hilpert, T. Markus, L. Singheiser, J. Power Sources 164 (2007) 578–589.
[23] S. Canovic, J. Froitzheim, R. Sachitanand, M. Nikumaa, M. Halvarsson, L.G. Johansson, J.E. Svensson, Surf. Coat. Technol. 215 (2013) 62–74.
[24] J. Froitzheim, S. Canovic, M. Nikumaa, R. Sachitanand, L.G. Johansson, J.E. Svensson, J. Power Sources 220 (2012) 217–227.
[25] J. Froitzheim, H. Ravash, E. Larsson, L.G. Johansson, J.E. Svensson, J. Electrochem. Soc. 157 (2010) B1295–B1300.
[26] J.G. Grolig, J. Froitzheim, J.E. Svensson, J. Power Sources 248 (2014) 1007–1013.
[27] J.W. Wu, C.D. Johnson, R.S. Gemmen, X.B. Liu, J. Power Sources 189 (2009) 1106–1113.
[28] C. Macauley, P. Gannon, M. Deibert, P. White, Int. J. Hydrogen Energy 36 (2011) 4540–4548.
[29] P. Gannon, M. Deibert, P. White, R. Smith, H. Chen, W. Priyantha, J. Lucas, V. Gorokhousky, Int. J. Hydrogen Energy 33 (2008) 3991–4000.
[30] A. Harthøj, T. Holt, P. Møller, J. Power Sources 281 (2015) 227–237.
[31] A. Magrasó, H. Falk-Windisch, J. Froitzheim, J.-E. Svensson, R. Haugsrud, Int. J. Hydrogen Energy 40 (2015) 8579–8585.
[32] J.G. Grolig, J. Froitzheim, J.-E. Svensson, J. Power Sources 284 (2015) 321–327.
[33] S.M. Technology, in.
[34] R. Sachitanand, M. Sattari, J.E. Svensson, J. Froitzheim, Int. J. Hydrogen Energy 38 (2013) 15328–15334.
[35] H.F. Windisch, J. Froitzheim, J.E. Svensson, Solid Oxide Fuel Cells 13 (Sofc-Xiii) 57 (2013) 2225–2233.
[36] R. Sachitanand, J.E. Svensson, J. Froitzheim, Oxid. Met. (2015) 1–17.
[37] M. Stanislowski, E. Wessel, K. Hilpert, T. Markus, L. Singheiser, J. Electrochem. Soc. 154 (2007) A295–A306.
[38] H. Falk-Windisch, J.E. Svensson, J. Froitzheim, J. Power Sources 287 (2015) 25–35.
[39] P. Huczkowski, S. Ertl, J. Piron-Abellan, N. Christiansen, T. Hofler, V. Shemet, L. Singheiser, W.J. Quadakkers, Mater High. Temp. 22 (2005) 253–262.